J Mater Sci: Mater Electron (2016) 27:10516–10524
DOI 10.1007/s10854-016-5142-9

Electric and magnetic properties of Y-type $Ba_2Mg_2Fe_{12}O_{22}$ hexaferrites with various Co doping

Meixia Wu[1,2] · Laijun Liu[3] · Xingsen Gao[2] · Zhongwu Liu[1]

Received: 30 March 2016 / Accepted: 6 June 2016 / Published online: 9 June 2016

Abstract Y-type hexaferrites $Ba_2Mg_{2-x}Co_xFe_{12}O_{22}$ ($x = 0.4$, 0.8, 1.2, 1.6) were synthesized by solid state reaction method. The impedance spectrum, AC conductivity, and dielectric properties were investigated at various temperatures and in a wide range of frequency. The dielectric properties and AC conductivity have been explained on the basis of space charge polarization and the electric exchange between Fe^{3+} and Fe^{2+} as well as the hole hopping between Co^{2+} and Co^{3+} ions at octahedral side. The complex impedance analysis indicates the existence of space charge and the presence of electrical processes at increased temperatures. The change of the activation energy obtained from $\ln f_{max}$ versus $1/T$ and $\ln\sigma_{dc}$ versus $1/T$ plots indicated that with increasing Co content, the transport mechanisms at low and high temperatures are different. Two magnetic phase transitions were observed in these samples and their transition temperatures increased with increasing Co^{2+} doping. High Co content suppresses the second magnetic structure transition under an applied magnetic field. For all samples, the room temperature coercivity is less than 20 Oe, while the saturation magnetization increases with increasing Co content. The present work provides a fundamental understanding of the dielectric and conductivity mechanism of Mg_2Y type hexaferrite, which is essential for microwave and electronic applications in the materials.

✉ Xingsen Gao
xingsengao@scnu.edu.cn

✉ Zhongwu Liu
zwliu@scut.edu.cn

[1] School of Materials Science and Engineering, South China University of Technology, Guangzhou 510640, China

[2] Institute for Advanced Materials and Laboratory of Quantum Engineering and Quantum Materials, South China Normal University, Guangzhou 510006, China

[3] Key Laboratory of New Processing Technology for Nonferrous Metal and Materials, Ministry of Education, College of Material Science and Engineering, Guilin University of Technology, Guilin 541004, China

1 Introduction

A variety of ferrites, including spinel ferrites and magnetoplumbite ferrites, exhibit excellent magnetic and electric properties, and have important applications in magnetic and electric devices. For examples, Fe_3O_4 [1], $CoFe_2O_4$ [2, 3] and Z-type [4], W-type [5], M-type [6] hexaferrites can be used as microwave absorbing materials based on their nature resonance loss and magnetic hysteresis loss. The polycrystalline Y-type hexaferrites also show high dielectric constants, low AC electrical conductivity, and low dielectric losses, which make them very useful for microwave applications and chip components [7–10]. The chemical formula of Y-type hexaferrite can be expressed in the general form of $(Ba,Sr)_2Me_2Fe_{12}O_{22}$ (Me = Co, Mg, Zn, Ni, Cu, etc.). Its structure belongs to space group $R\bar{3}m$ and is constructed from the basic units of hexagonal barium ferrites and cubic spinel ferrites [7].

The dielectric and conductivity properties are the most important properties of the polycrystalline Y-type hexaferrites, which depend on the prepared method, ion distribution, doping elements and so on [11]. The dielectric constants for Y-type hexaferrites can be as high as 10^4–10^6 and show dispersion at low frequencies [12–14]. These phenomena were discussed based on the Maxwell–Wagner model [15, 16] and Koop's phenomenological theory [17] in connection with the inhomogeneous structure of sample. For good understanding the mechanism of electric conduction and dielectric polarization in hexaferrites, the

experimental measurements of the dielectric constant, impedance spectrum, AC conductivity and activation energy can provide valuable information on the behavior of the free and localized charge carriers [18].

Up to now, many investigations have been focused on the dielectric properties and conductivity properties of Y-type hexaferrite, such as the Zn_2Y hexaferrite [19, 20], Co_2Y hexaferrite [21–23], and Ni_2Y hexaferrite [10, 13, 24]. However, there is few work related to the dielectric and conductivity properties of Mg_2Y hexaferrite. It was reported that $Ba_2Mg_2Fe_{12}O_{22}$ (Mg_2Y) hexaferrite is a multiferroic material which exhibits the highest controllability of ferroelectric polarization under the weak magnetic field, and the polarization can be reversed by the magnetic field switching [25, 26]. Therefore, in order to further understand the interesting properties of Mg_2Y hexaferrite, it is important to investigate the dielectric and conductivity properties of this ferrite.

In this work, we prepared the Mg_2Y-type $Ba_2Mg_{2-x}Co_xFe_{12}O_{22}$ hexaferrites with various compositions by solid state reaction method. The dielectric properties were studied at a wide frequency region, from 40 Hz to 1 MHz. The conductivity, complex impedance spectra and magnetic properties at different temperatures were investigated. This work aims to give a valuable understanding of the conductivity behavior of Mg_2Y-type hexaferrite.

2 Experimental

Polycrystalline samples of Mg_2Y-type hexaferrties $Ba_2Mg_{2-x}Co_xFe_{12}O_{22}$ ($x = 0.4$, 0.8, 1.2, and 1.6) were synthesized by the traditional solid state reaction method as our previous work [27]. The raw materials of $BaCO_3$ (99 %), MgO (98 %), Co_3O_4 (99 %) and Fe_2O_3 (99.99 %) with desired ratios were thoroughly mixed by ball milling with agate balls in ethanol for 2 h. The mixtures were dried and pre-sintered at 1000 °C for 6 h in air. After that, they were milled again and dry pressed into pellets with approximately 11.5 mm in diameter and 2–3 mm in thickness. Finally, the pellets were sintered at 1200 °C for 16 h followed by annealing at 1000 °C for 10 h in air.

The phase purity was detected by using an X-ray diffractometer (XRD) (Cu-$K\alpha$1, 1.54059 Å, Model X'Pert PRO, PANalytical, Almelo, Netherlands) at room temperature. The phase can be assigned to the Y-type hexaferrite as shown in Fig. 1. Vibrating sample magnetometer (VSM, Quantum Design's PPMS-9T) was used to measure the magnetization curves and magnetic hysteresis loops of the samples at various temperatures. The temperature dependence of magnetization was measured in the temperature range of 30–380 K. For the electrical measurement, the samples were polished into thin plates with a thickness of

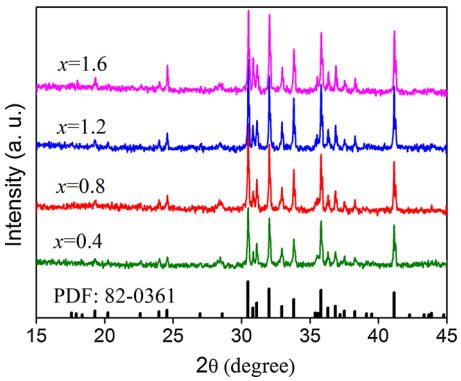

Fig. 1 Powder X-ray diffraction patterns of $BaMg_{2-x}Co_2Fe_{12}O_{22}$ samples

$\sim$0.5 mm, and conductive silver paste was used on both sides in order to create good electrodes. A computer-controlled impedance analyzer (Agilent 4294A, Agilent Technologies, Santa Clara, USA) was used to measure the dielectric properties in the frequency range from 40 Hz to 1 MHz and the impedance spectra at various temperatures with a set of temperature control facilities.

3 Results and discussion

3.1 Complex impedance spectrum

The complex impedance spectroscopy is a very well known technique to describe the electrical properties of polycrystalline electroceramics. The grain and grain boundary contributions to the electrical properties of dielectric materials can be analyzed by using an equivalent circuit which consists of two parallel RC circuits, R_gC_g and $R_{gb}C_{gb}$, where R_gC_g represents the grain boundary circuit corresponding to the low frequency response, while $R_{gb}C_{gb}$ is the grain circuit corresponding to high frequency response.

For the prepared $Ba_2Mg_{2-x}Co_xFe_{12}O_{22}$ samples, the complex impedance spectra in a wide range of frequencies (40 Hz–1 MHz) at different temperatures (300–430 K) were investigated. The variations of real (Z'), imaginary (Z''), and Z' versus Z'' part of impedance at selected temperatures are shown in Figs. 2, 3 and 4.

In Fig. 2, the real parts of impedance (Z') of all samples exhibit the low frequency dispersion. With increasing temperature, all samples show a temperature dependent Z' plateau at low frequencies. This plateau indicates the dc conductivity of the samples, appears to broaden towards high frequency side with the increases in temperature and in x value. Also, Z' values decrease with increasing temperature and frequency, and finally merged in the high frequency region for all samples. The decrease of Z' may

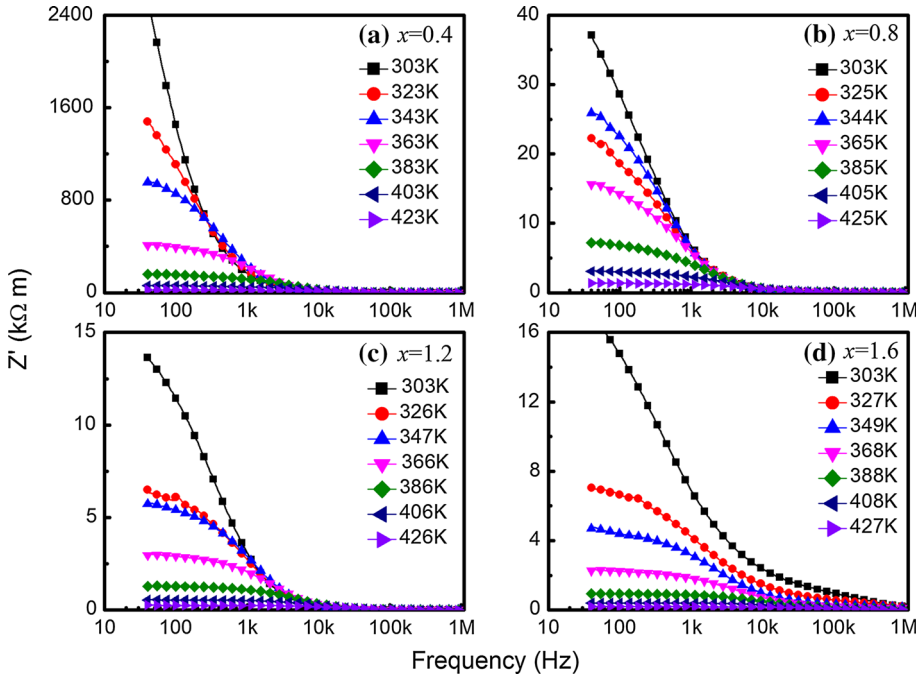

Fig. 2 Frequency dependence of the real part Z' of impedance for $BaMg_{2-x}Co_2Fe_{12}O_{22}$ at different temperatures

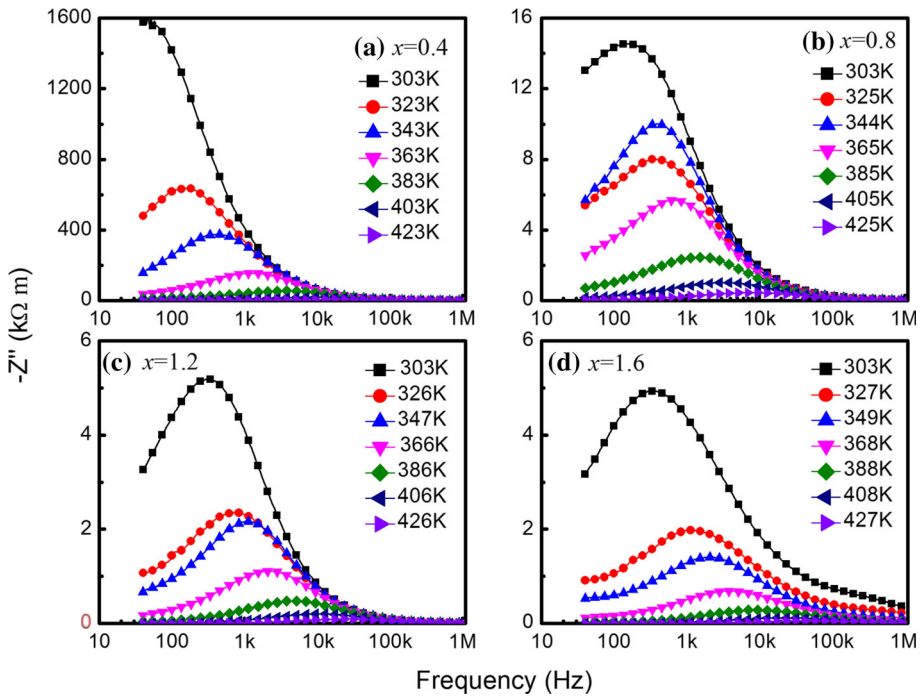

Fig. 3 Frequency dependence of the imaginary part Z'' of impedance for $BaMg_{2-x}Co_2Fe_{12}O_{22}$ at different temperatures

be due to the increasing ac conductivity with the temperature and frequency. The merged Z' suggests a possible release of space charge and a consequent lowering of the barrier properties in the materials [28].

Figure 3 shows the plot of imaginary part of impedance (Z'') versus frequency at various temperatures. All samples show a loss peak and the peak position shifts to high frequency side and the peak value decreases with increasing temperature. This type of impedance spectrum is probably due to the presence of space charge in the sample and ensures the temperature dependent relaxation process [29]. The appearance of peak in the loss spectrum is an indication of the beginning of electrical relaxation in the material [28]. Therefore, it can be concluded that the space charge and electrical relaxation may exist in all samples below the room temperature. At high frequency region, the spectra

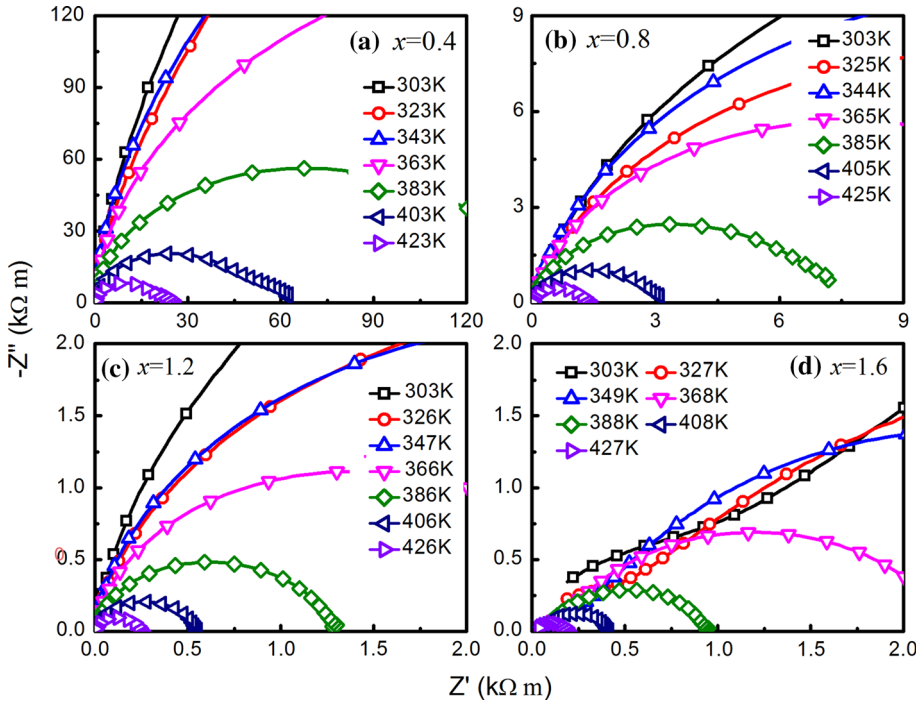

Fig. 4 Real (Z') versus imaginary (Z'') part of impedance at different measurement temperatures of $BaMg_{2-x}Co_2Fe_{12}O_{22}$ samples

merged together irrespective of temperature for all samples, which indicates the space charge release at high frequency. Another feature of Fig. 3 is the asymmetric broadening of the loss peaks for all samples, which is an evidence of the presence of electrical processes [28], i.e. the electric exchange between Fe^{3+} and Fe^{2+} and hole exchange between Co^{2+} and Co^{3+}.

The Z' versus Z'' plots for the samples are displayed in Fig. 4. Clear semicircles can be found for all samples at the selected temperatures. The center of these semicircles are all located below the real axis (Z'), indicating a non-Debye relaxation. There are two semicircles (or its tendency) presented for $x = 0.4$ sample, while only one for x>0.4 samples. The high frequency semicircle is attributed to the grain effect while the low frequency semicircle results from the grain boundary. The presence of two semicircular arcs in the impedance spectrum for $x = 0.4$ sample indicates the presence of both bulk and grain boundary contributions to its overall electrical properties.

The relaxation frequency at the apex of the Z' versus Z'' semicircle is an intrinsic characteristic frequency of the ceramics, and it fulfills the condition $2\pi f_{max}RC = 1$. The relaxation activation energies E_{rel} can be determined from the frequency using the Arrhenius law, $\omega = 2\pi f = \omega_0 \exp[-E_{rel}/k_BT]$, where ω_0 is the preexponential factor and k_B is the Boltzmann constant. The obtained E_{rel} values are shown in Table 1. Figure 5 shows a non-linear relationship for the plot of $\ln f_{max} - 1/T$ except for the sample of $x = 0.4$. The non-linear behavior can be described by various data regions, including low temperature region, define as region I, and high temperature region, as region II. Therefore, two activation energies exist for x>0.4 samples. The activation energy in region I is smaller than that in region II, which indicates the relaxation processes are attributed to different response mechanisms. In region I, the values of E_{rel} for $x = 0.8$ and 1.2 samples are 0.33 and 0.32 eV, respectively, while for $x = 1.6$ the value is 0.45 eV. This level of E_{rel} values indicates that the relaxation carriers are due to the electron hopping between $Fe^{3+} \leftrightarrow Fe^{2+}$ and hole transfer between $Co^{2+} \leftrightarrow Co^{3+}$ (Refs. [12, 20, 22]). In region II, the values of E_{rel} are 0.53–0.62 eV for all samples, which are comparable to those obtained in other works [30, 31], indicating that the relaxation carries are the oxygen vacancies [31–34].

3.2 AC conductivity analysis

Figure 6 shows the ac conductivity as a function of frequency at different temperatures. For all samples, the frequency independent plateau was found at the low frequency region and extends to higher frequencies with increasing temperature. This plateau is attributed to the long-range translational motion of ions contributing to dc conductivity. At high frequency, the AC conductivity increases exponentially with increasing frequency due to the increasing hopping of carriers. For $x = 1.6$ sample, a step-like behavior was found below 368 K in the $\sigma_{ac} - f$ plots, indicating the multiple relaxation process for the sample. With increasing Co^{2+} ion number, the hole transition between $Co^{2+} \leftrightarrow Co^{3+}$ becomes dominant. So it can be concluded that, the multiple relaxation process for $x = 1.6$ sample at the low temperatures is due to the oxygen vacancies and the hole transition between $Co^{2+} \leftrightarrow Co^{3+}$.

Table 1 Activation energy and magnetic properties measured at 300 K

Sample	E_{rel} (eV)		E_{con} (eV)		Magnetic transition temperature (K)		M_S (emu/g)	H_C (Oe)
	I	II	I	II	T_1	T_2		
$x = 0.4$	0.62	0.21	0.61	50	200	24.22	14.9	
$x = 0.8$	0.33	0.53	0.24	0.54	77	182	26.18	18.3
$x = 1.2$	0.32	0.53	0.27	0.55	90	203	28.85	16.7
$x = 1.6$	0.45	0.58	0.35	0.56	92	226	30.09	20.1

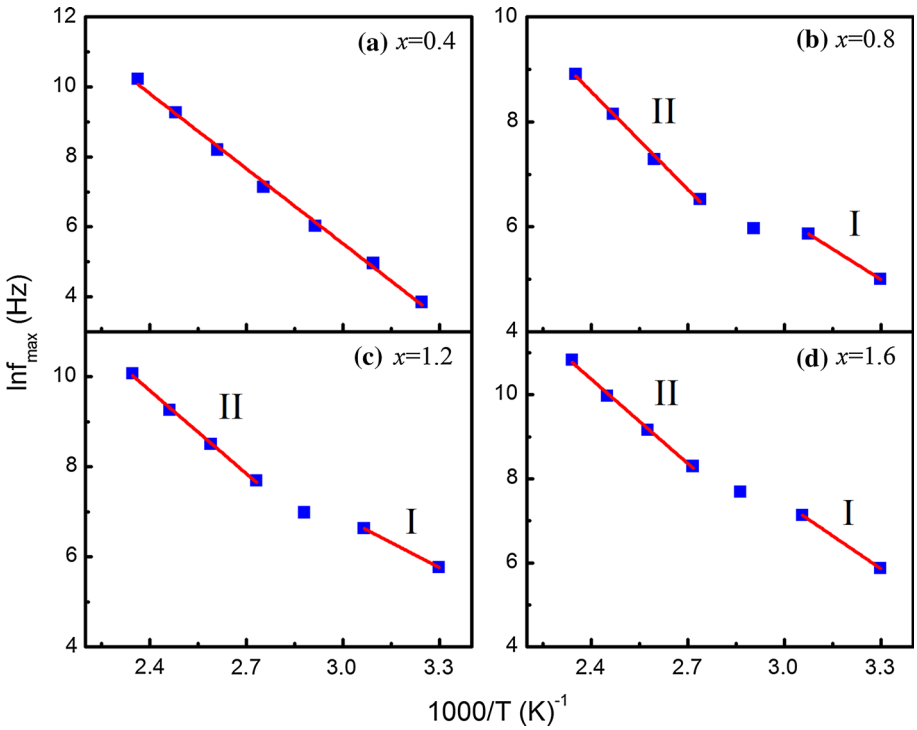

Fig. 5 Arrhenius plots of f_{max} (peak) versus 1000/T of $BaMg_{2-x}Co_2Fe_{12}O_{22}$ samples

The frequency behavior of conductivity can be investigated based on the universal power law [35], $\sigma'_{ac} = \sigma_{dc} + a\omega^n$. The first term σ_{dc} is the dc electrical conductivity, which follows an Arrhenius form, $\sigma_{dc} = \sigma_0 \exp(-E_a/k_BT)$. The conductivity activation energy E_{con} can be calculated from the plot of $\ln\sigma_{dc} - 1/T$, and the values are also shown in Table 1. The data in Fig. 7 for all samples show non-linear relationship, which can also be defined as region I (low-temperature region) and region II (high-temperature region). As for the case of relaxation, the conductivity activation energies for all samples in region I are smaller than those in region II. In region I, the activation energy increases with the increasing Co^{2+} ion number. The values for $x \leq 1.2$ samples are 0.21–0.27 eV, and that for $x = 1.6$ sample is 0.35 eV. These values are comparable to the relaxation activation energies in region I, and indicates the relaxation and conductivity processes may be attributed to the same type of carries, i.e. the electron hopping between $Fe^{3+} \leftrightarrow Fe^{2+}$ and hole transfer between $Co^{2+} \leftrightarrow Co^{3+}$. Therefore, with increasing Co^{2+} ion concentration, the electron hopping between $Fe^{3+} \leftrightarrow Fe^{2+}$ and hole transfer between $Co^{2+} \leftrightarrow Co^{3+}$ become the dominant mechanism. In region II, E_{con} values for all samples are 0.54–0.61 eV, close to that of relaxation, indicating that the relaxation and conductivity processes are attributed to the oxygen vacancies.

Therefore, it can be concluded that, at low temperatures, the carries for relaxation and conductivity are the $Fe^{3+} \leftrightarrow Fe^{2+}$ and $Co^{2+} \leftrightarrow Co^{3+}$, while at high temperatures, oxygen vacancies become the dominant carrier for the relaxation and conductivity. However, for the abundant Co-doping sample ($x = 1.6$), $Co^{2+} \leftrightarrow Co^{3+}$ may be the dominant carriers since the E_{rel} and E_{con} are 0.45 and 0.35 eV, respectively.

3.3 Dielectric properties

As shown in Fig. 8a, the dielectric constants (ε') versus frequency plots of $Ba_2Mg_{2-x}Co_xFe_{12}O_{22}$ samples clearly show the large ε' values for the samples with relatively high

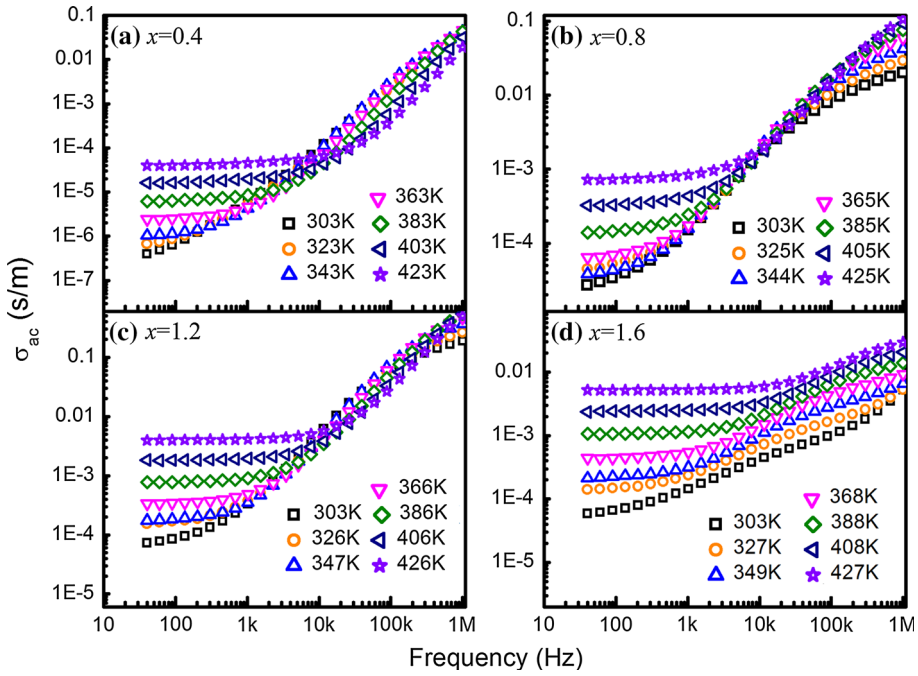

Fig. 6 Frequency dependence of the real part of AC conductivity σ'_{ac} at different temperature

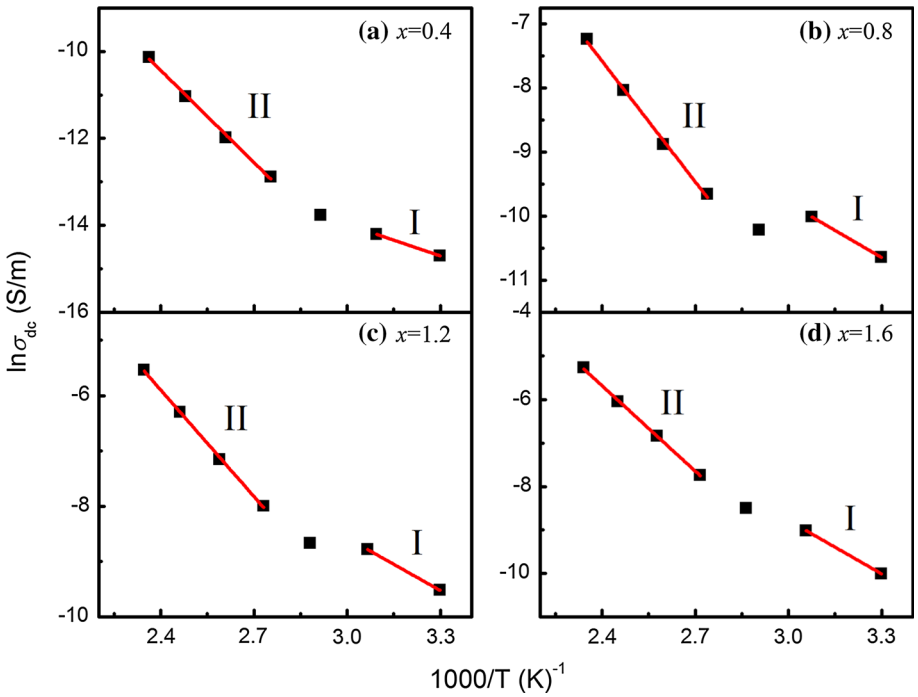

Fig. 7 Temperature dependence of dc conductivity and its fitting curve from Arrhenius law

Co-doping at the low frequency. With increasing the frequency, ε' decreases continuously. For the Co^{2+}-containing $Ba_2Mg_{2-x}Co_xFe_{12}O_{22}$ samples, $Co^{2+} \rightarrow Co^{3+}+e^-$ will occur. As analyzed in the conductivity behavior, the carries contributed to the conductivity process are electric exchanges between $Fe^{3+} \leftrightarrow Fe^{2+}$ and hole hopping between $Co^{2+} \leftrightarrow Co^{3+}$. Since the mechanism of the polarization process in ferrites is similar to that of the conduction process [36, 37], it can be assumed that the electric exchange between Fe^{2+} and Fe^{3+} gives rise to the displacement of the local charges in the direction of the external field while the hole transfer between Co^{2+} and Co^{3+} will give rise to displacement of the holes in the opposite direction of the external field, which are the main origin of polarization [13] and contribute to the high dielectric constant at low frequency. With increasing Co^{2+}

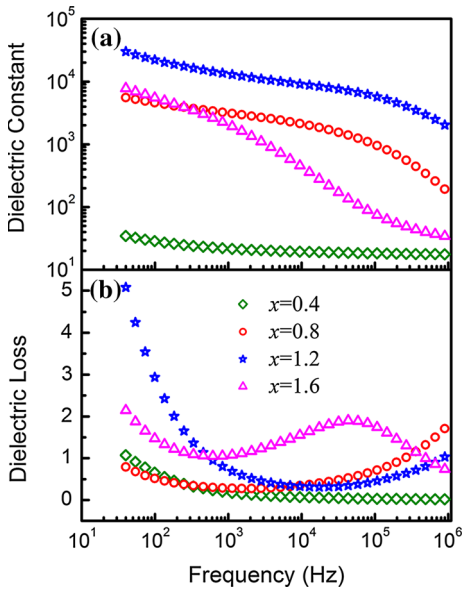

Fig. 8 Frequency dependence of **a** dielectric constant (ε') and **b** dielectric loss (tanδ) of $BaMg_{2-x}Co_2Fe_{12}O_{22}$ samples at room temperature

ion concentration, the exchange interaction of $Co^{2+} + Fe^{3+} \leftrightarrow Co^{3+} + Fe^{2+}$ become more active [12]. Therefore, the dielectric constant increases with increasing cobalt content. At high frequency, the electric exchange $Fe^{3+} \leftrightarrow Fe^{2+}$ and hole exchange $Co^{2+} \leftrightarrow Co^{3+}$ cannot follow the change of the applied field, leading to the decrease of dielectric constant.

The dependence of dielectric loss (tanδ) on the frequency is shown in Fig. 8b. All samples show dispersion behavior. The dielectric loss of $x = 0.4$ sample is very low due to the small dielectric constant value. For $x = 0.8$ and 1.2 samples, the dielectric loss at high frequency shows an increasing tendency. This may be due to the existence of a dielectric peak at higher frequencies (out-of the observed window). While for $x = 1.6$ sample, a dielectric loss peak exhibits at lower frequency (in the measure frequency). In other words, with increasing Co content, the dielectric loss peak shifts to low frequency side. Therefore, it can be roughly concluded that the hopping frequency of $Co^{2+} \leftrightarrow Co^{3+}$ is smaller than that of $Fe^{3+} \leftrightarrow Fe^{2+}$. The dielectric loss peak for the $x = 1.6$ sample may result from the collective contributions of both $Co^{2+} \leftrightarrow Co^{3+}$ and $Fe^{3+} \leftrightarrow Fe^{2+}$ type of charge carriers [38]. A peak exhibits when the jumping frequency of electrons exchange between Fe^{2+} and Fe^{3+} and hole transfer between Co^{3+} and Co^{2+} in octahedral sites are equal to the frequency of the applied AC field.

3.4 Magnetic studies

The magnetic phase transition temperatures in $Ba_2Mg_{2-x}Co_xFe_{12}O_{22}$ ($x = 0.4$, 0.8, 1.2, 1.6) were determined from the temperature dependence of magnetization measured after zero field cooling (ZFC) in an applied magnetic field of 0.05 T (Fig. 9). Two magnetic phase transitions can be clearly seen from the dM/dT versus T plot, and the transition temperatures are marked as T_1 and T_2, respectively. For $Ba_2Mg_2Fe_{12}O_{22}$, it was reported [25, 39] that the magnetic ordering changes from collinear ferrimagnetic structure to a proper-screw spin phase at the temperature around 195 K, and from the screw spin phase to a longitudinal conical spin phase at around 50 K. Similarly, for our samples, the transition temperature T_1 may represent the temperature for the magnetic ordering change from screw to conical structure, while T_2 represents the temperature for the change from collinear to screw structure. The magnetic transition temperatures for all samples are given in Table 1. All transition temperatures increase with increasing Co content, which results from the fact that Co^{2+} ions can contribute to the enhancement of the magnetic ordering temperatures [40]. However, for $x = 0.8$ sample, the magnetic transition temperature T_2 is less than that for the $x = 0.4$ sample. The reason for the decrease of this temperature is still unknown.

Figure 10 shows the magnetic hysteresis loops measured with an applied field 4 T at different temperatures. The coercivity (H_C) and the saturation magnetization (M_S) at 300 K were shown in Table 1. H_C values for all samples are very small (less than 20 Oe), which means the Co^{2+} ions make a litter effect on the coercivity at 300 K. However, M_S increases with the increasing Co content. As we known, the Co^{2+} ions are the magnetic ions and have the magnetic moment of 3 μ_B, whereas the Mg^{2+} ions are non-magnetic ions and do not have any magnetic moment. Both of them are preferred to occupy the octahedral side. The increase in magnetic Co^{2+} ions replaces of non-magnetic Mg^{2+} ions results in an enhancement of magnetization. In addition, the stepwise changes in M–H curve for hexaferrites was reported to indicate the H-induced phase transitions [25, 26, 41, 42]. It is clear in Fig. 10 that all samples shown the stepwise character in the M–H curve at the selected measuring temperatures. One stepwise change can be found at around 0.1 T. Clearly, Co substitution has no significant effect on this field. This change corresponds to the magnetic transition from the slanted longitudinal conical to transverse conical phase [42]. For $x = 0.04$ sample,

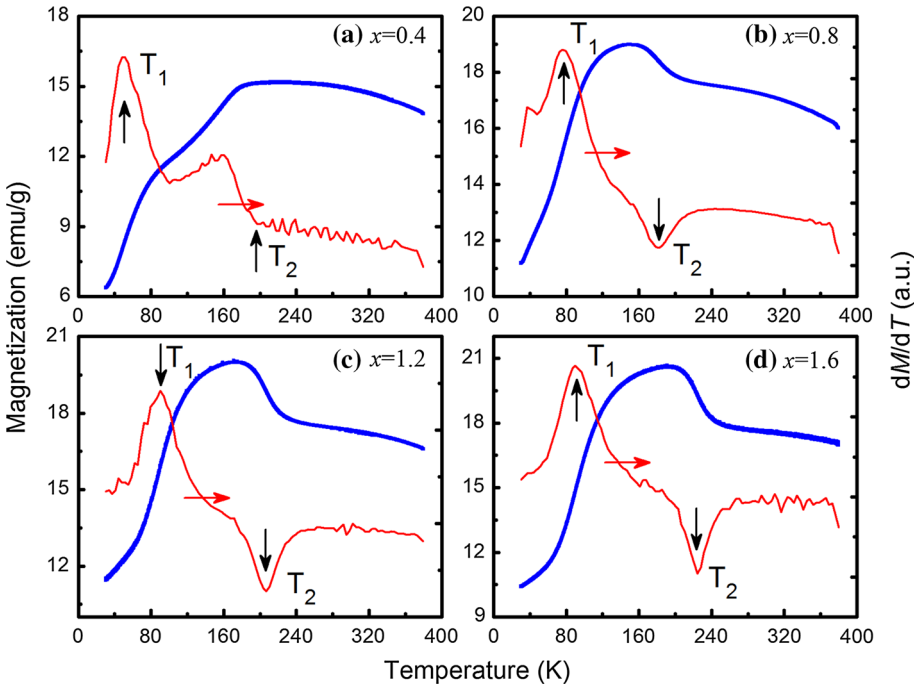

Fig. 9 Temperature dependence of magnetization and its dM/dT for $BaMg_{2-x}Co_2Fe_{12}O_{22}$ samples

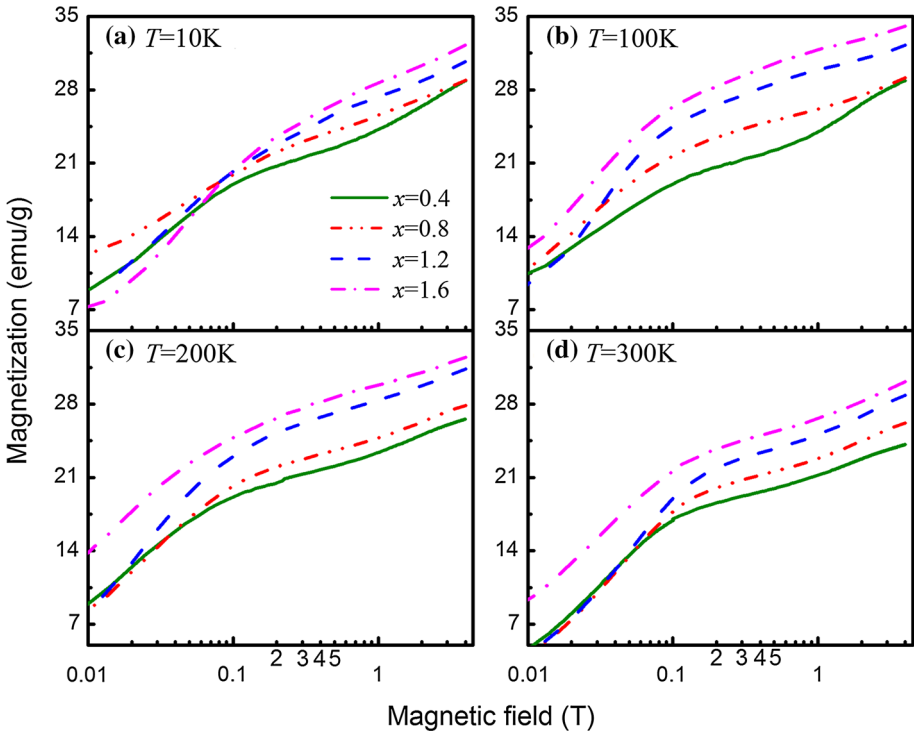

Fig. 10 Magnetic field dependence of magnetization for $BaMg_{2-x}Co_2Fe_{12}O_{22}$ samples

another stepwise change was found at around 1 T, and it gradually disappear with increasing temperature. This change indicates the ferroelectric phase transition between FE2 and FE3 phases, which is only 0.25 T for $Ba_2Mg_2Fe_{12}O_{22}$ [42].

4 Conclusion

In summary, Co-doped Y-type hexaferrites $Ba_2Mg_{2-x}Co_xFe_{12}O_{22}$ (x = 0.4, 0.8, 1.2, 1.6) were prepared by solid state reaction method. The conductivity and relaxation

process are contributed to different carries at low and high temperatures. $Co^{2+} \leftrightarrow Co^{3+}$ and $Fe^{3+} \leftrightarrow Fe^{2+}$ types of charge carriers play a major role at low temperature while oxygen vacancies show a significant effect at high temperature. With increasing Co^{2+} ion concentration, $Co^{2+} \leftrightarrow Co^{3+}$ becomes the dominant carrier for relaxation and conductivity process at low temperature. The dielectric polarization process in these ferrites is similar to that of the conduction process, and the electric exchange between Fe^{2+} and Fe^{3+} and the hole transfer between Co^{2+} and Co^{3+} are responsible for the high dielectric constant at low frequency side. Two magnetic phase transitions are observed in all samples, one corresponds to the magnetic change from ferrimagnet to proper screw magnetic structure, and the other represents the change from screw to longitudinal conical structure. With increasing Co^{2+} ions, all the magnetic transition temperatures and the magnetization increase. However, Co^{2+} ions make a litter effect on the coercivity at 300 K. The present results give a fundamental understanding of the dielectric and conductivity mechanism of Mg_2Y type hexaferrite, which exhibits potential use in microwave magnets and magnetoelectric materials.

Acknowledgments Z.W.L. thanks the Program for New Century Excellent Talents in University (Grant No. NCET-11-0156) and the Fundamental Research Funds for the Central Universities (Grant No. 2015ZP030). X.S.G. thanks the Natural Science Foundation of China (Grant Nos. 51031004, 51272078) and the Guangdong National Science Foundation (S2012010008124).

References

1. X. Huang, Y. Chen, J. Yu, J. Zhang, T. Sang, G. Tao, H. Zhu, J. Mater. Sci.: Mater. Electron. **26**, 3474–3478 (2015)
2. X. Huang, J. Zhang, W. Rao, T. Sang, B. Song, C. Wong, J. Alloys Compd. **662**, 409–414 (2016)
3. X. Huang, J. Zhang, W. Wang, T. Sang, B. Song, H. Zhu, W. Rao, C. Wong, J. Magn. Magn. Mater. **405**, 36–41 (2016)
4. B. Li, Y. Shen, Z. Yue, C. Nan, J. Magn. Magn. Mater. **313**, 322–328 (2007)
5. R.A. Khan, S. Mizukami, A.M. Khan, B. Ismail, A.R. Khan, T. Miyazaki, J. Alloys Compd. **637**, 197–202 (2015)
6. X. Huang, J. Zhang, Z. Liu, T. Sang, B. Song, H. Zhu, C. Wong, J. Alloys Compd. **648**, 1072–1075 (2015)
7. J. Smit, H.P.J. Wijn, *Ferrites* (Philips' Technical Library, Eindhoven, 1959)
8. Y. Bai, J. Zhou, Z. Gui, L. Li, J. Magn. Magn. Mater. **246**, 140–144 (2002)
9. H. Kwon, J. Shin, J. Oh, J. Appl. Phys. **75**, 6109–6111 (1994)
10. M. El Hiti, A.A. El Ata, J. Magn. Magn. Mater. **195**, 667–678 (1999)
11. A. Shaikh, S. Bellad, B. Chougule, J. Magn. Magn. Mater. **195**, 384–390 (1999)
12. M. Wu, W. Zhong, X. Gao, L. Liu, Z. Liu, J. Appl. Phys. **116**, 224103 (2014)
13. A.A. El Ata, S. Attia, J. Magn. Magn. Mater. **257**, 165–174 (2003)
14. G. Pires, H. Rodrigues, J. Almeida, E. Sancho, J. Góes, M. Costa, J. Denardin, A. Sombra, J. Alloys Compd. **493**, 326–334 (2010)
15. J.C. Maxwell, *A Treatise on Electricity and Magnetism* (Clarendon Press, Oxford, 1881)
16. K. Wagner, Ann. Phys. **345**, 817 (1913)
17. C. Koops, Phys. Rev. **83**, 121 (1951)
18. M. El Hiti, J. Magn. Magn. Mater. **164**, 187–196 (1996)
19. S. Kamba, V. Goian, M. Savinov, E. Buixaderas, D. Nuzhnyy, M. Maryško, M. Kempa, V. Bovtun, J. Hlinka, K. Knížek, J. Appl. Phys. **107**, 104109 (2010)
20. S. Hirose, K. Haruki, A. Ando, T. Kimura, J. Am. Ceram. Soc. **98**, 2104–2111 (2015)
21. M. Costa, G.P. Júnior, A. Sombra, Mater. Chem. Phys. **123**, 35–39 (2010)
22. I. Ali, M. Islam, M.N. Ashiq, H.M. Khan, M.A. Iqbal, M. Najam-Ul-Haq, Mater. Res. Bull. **49**, 338–344 (2014)
23. I. Ali, M. Islam, M.N. Ashiq, M.A. Iqbal, M. Awan, S. Naseem, J. Alloys Compd. **599**, 131–138 (2014)
24. M. Irfan, M. Islam, I. Ali, M.A. Iqbal, N. Karamat, H.M. Khan, Curr. Appl. Phys. **14**, 112–117 (2014)
25. S. Ishiwata, Y. Taguchi, H. Murakawa, Y. Onose, Y. Tokura, Science **319**, 1643–1646 (2008)
26. K. Taniguchi, N. Abe, S. Ohtani, H. Umetsu, T.-H. Arima, Appl. Phys. Express **1**, 031301 (2008)
27. M. Wu, X. Gao, Z. Liu, J. Am. Ceram. Soc. **98**, 2498–2502 (2015)
28. A. Kumar, B. Singh, R. Choudhary, A.K. Thakur, Mater. Chem. Phys. **99**, 150–159 (2006)
29. B. Tiwari, R. Choudhary, J. Alloys Compd. **493**, 1–10 (2010)
30. M. Costa, G. Pires Jr., A. Terezo, M. Graca, A. Sombra, J. Appl. Phys. **110**, 034107 (2011)
31. S. Hussain, M. Anis-ur-Rehman, A. Maqsood, M. Awan, J. Cryst. Growth **297**, 403–410 (2006)
32. C. Ang, Z. Yu, L. Cross, Phys. Rev. B **62**, 228 (2000)
33. S. Hussain, A. Maqsood, J. Alloys Compd. **466**, 293–298 (2008)
34. G. Li, Z. Chen, X. Sun, L. Liu, L. Fang, B. Elouadi, Mater. Res. Bull. **65**, 260–265 (2015)
35. A.K. Jonscher, *Dielectric Relaxation in Solids* (Chelsea Dielectrics Press, London, 1983)
36. L.I. Rabinkin, Z.I. Novikova, Ferrites. Minsk (1960), p. 146
37. K. Iwauchi, Jpn. J. Appl. Phys. **10**, 1520 (1971)
38. N. Rezlescu, E. Rezlescu, Phys. Status Solidi A **23**, 575–582 (1974)
39. N. Momozawa, Y. Yamaguchi, M. Mita, J. Phys. Soc. Jpn. **55**, 1350–1358 (1986)
40. H.B. Lee, S.H. Chun, K.W. Shin, B.-G. Jeon, Y.S. Chai, K.H. Kim, J. Schefer, H. Chang, S.-N. Yun, T.-Y. Joung, Phys. Rev. B **86**, 094435 (2012)
41. N. Momozawa, Y. Yamaguchi, H. Takei, M. Mita, J. Phys. Soc. Jpn. **54**, 3895–3903 (1985)
42. S. Ishiwata, D. Okuyama, K. Kakurai, M. Nishi, Y. Taguchi, Y. Tokura, Phys. Rev. B **81**, 174418 (2010)